JOURNAL OF MATERIALS SCIENCE 16 (1981) 1223–1232

Effect of structure on the Young's modulus of Al–Cu–Ni alloys

HALA A. HAFEZ
Department of Production Engineering, Ain Shams University, Cairo, Egypt

MAHMOUD M. FARAG
Department of Materials Engineering, American University in Cairo, Cairo, Egypt

Experimental measurements of the dynamic Young's modulus of a wide range of wrought Al–Cu–Ni alloy compositions have shown this property to depend not only on the volume fraction of the phases present in the alloy but also on the microstructure. The results can be described by the simple relationship:

$$E = 76.6 + 94.6\,V_d - 1.3d + 0.06\lambda$$

where E is Young's modulus of the alloy (in GN m^{-2}), V_d is the volume fraction of all the dispersed phases, and d and λ are the respective average particle size and mean free path of all dispersed phases (in μm). In view of the wide range of alloys tested in the present work, the above equation is expected to apply reasonably well to most wrought aluminium alloys.

1. Introduction

Although a large number of investigations have been reported on the relation between Young's modulus and the composition of alloys [1–6], only a few attempts have been made to correlate this important property to the microstructure of the alloys [7]. The literature also contains many accurate theoretical formulae for the prediction of the Young's moduli of alloys in terms of their Poisson's ratio, shear modulus and bulk modulus of the constituent phases [8–11]. However, the application of such formulae to different alloys has been limited by the lack of information about the necessary physical properties. This has led, because of their simplicity, to the wide use of the following approximate formulae:

$$E_c = E_1V_1 + E_2V_2 + E_3V_3 + \ldots + E_nV_n; \quad (1)$$

$$\frac{1}{E_c} = \frac{V_1}{E_1} + \frac{V_2}{E_2} + \frac{V_3}{E_3} + \ldots + \frac{V_n}{E_n}, \quad (2)$$

where $E_c, E_1, E_2 \ldots E_n$ are the Young's moduli of the alloy and of the alloy phases, Phase 1, Phase 2, ... Phase n, respectively, and $V_1, V_2, \ldots V_n$ are the volume fractions of Phase 1, Phase 2, ... Phase n, respectively. Equation 1 assumes equal strain in all phases and gives an upper boundary value of Young's modulus; Equation 2 assumes equal stress in all phases and gives a lower boundary value. An interpolated formula is often used for alloys containing a dispersion, Phase 1, in a matrix, Phase 2:

$$E_c = E_2\left[\frac{1 + 2V_1\left(\frac{1 - E_2/E_1}{2E_2/E_1 + 1}\right)}{1 - V_1\left(\frac{1 - E_2/E_1}{2E_2/E_1 + 1}\right)}\right] \quad (3)$$

None of the above formulae take into account the size or morphology of the phases in the alloy; this could lead to inaccuracies of prediction since several investigators have shown that Young's modulus is structure sensitive [12–15].

The present work is an attempt to correlate Young's modulus and structure for a variety of wrought alloys in the aluminum-rich corner of the Al–Cu–Ni system.

0022–2461/81/051223–10$03.00/0

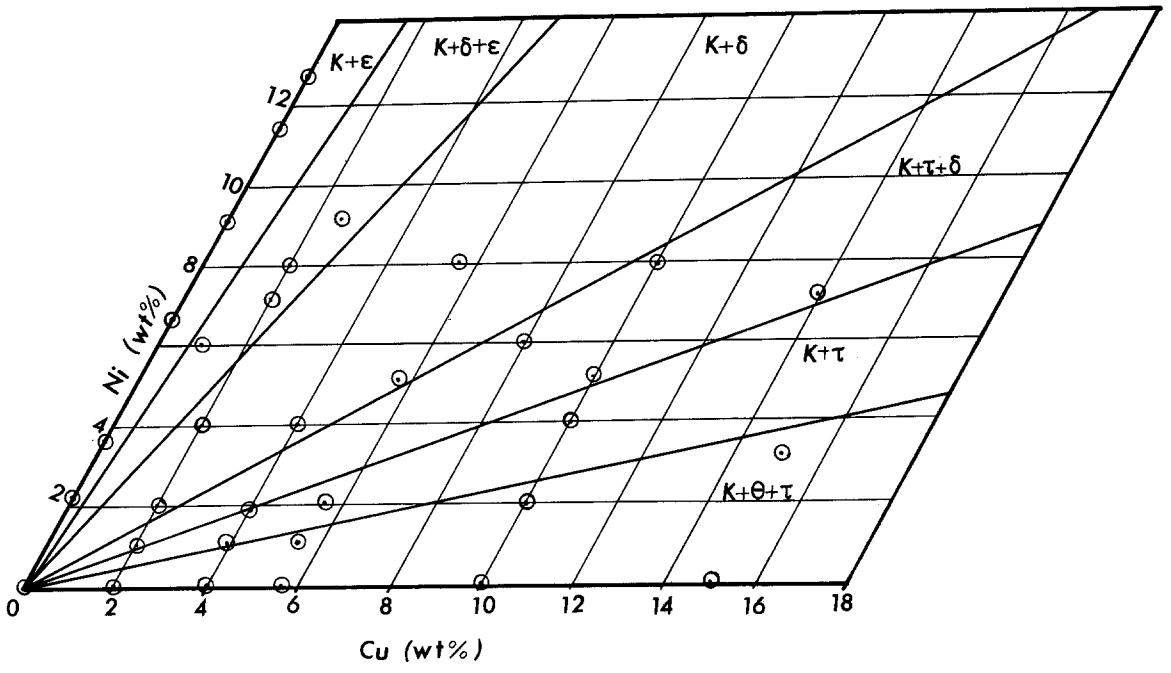

Figure 1 Diagram showing the aluminium-rich corner of the Al–Cu–Ni phase diagram indicating the nominal locations of the alloys investigated.

2. Experimental procedure

The Al–Cu–Ni alloys used in the present work were prepared from commercial purity (99.5%) aluminum, pure (99.95%) copper, and Al–19.49 wt% Ni commercial master alloy with an impurity content of 0.46%. 32 alloys were prepared with the nominal compositions shown in Fig. 1. Alloy rods, 9.5 mm in diameter and 150 mm in length, were cast and then homogenized at 375° C for 7 days. The rods were then cold swaged to 2.1 mm diameter and then annealed for 3 h at 375° C.

Metallographic specimens were prepared by polishing and etching using 10 wt% NaOH solution for 5 sec at 70° C. With this etchant, θ ($Cu\ Al_2$) and ϵ (Al_3Ni) appear brown, τ (Al_7Cu_4Ni) is outlined unattacked, and δ $(CuNi)_2Al_3$ appears as dark grey (see Fig. 1). Quantitative metallographic analyses were carried out using standard techniques for particle size, d, and volume fraction, V, determination. The mean free path, λ, was taken as

$$\lambda = \frac{2(1-V)d}{3V} \tag{4}$$

and the interparticle spacing, D, was taken as

$$D = \lambda + d. \tag{5}$$

The Young's modulus was measured using a modification of the dynamic technique described by Baveja [16]. In this technique one end of the specimen is fixed while a small permanent magnet is rigidly attached to the other end and is set into vibration by the action of an alternating magnetic field, as shown in Fig. 2. The frequency of the magnetic field was varied by means of an audio oscillator until resonance occurred in the specimen–magnet system. The resonance frequency was detected by a search coil connected to an oscilloscope.

The dynamic Young's modulus was calculated from the formula

$$E_c = \frac{\rho\omega^2 l^4}{Z^4 k^2}, \tag{6}$$

where ρ is the density of the alloy, l is the vibrating length of the specimen, ω is the natural angular frequency of the fundamental mode of vibration of the loaded specimen, k is the radius of gyration of the cross-section of the specimen, and Z is defined as

$$Z^4 = \frac{210}{A}\left\{B - \left(B^2 - \frac{4A}{35}\right)^{1/2}\right\}, \tag{7}$$

where

$$A = 1 + 8c + 168d + 420cd + 56\frac{cL}{l} + 168\frac{cL^2}{l^2} - 168\frac{cgL}{l^2\omega^2} - 420\frac{c^2gL}{l^2\omega^2} \tag{8}$$

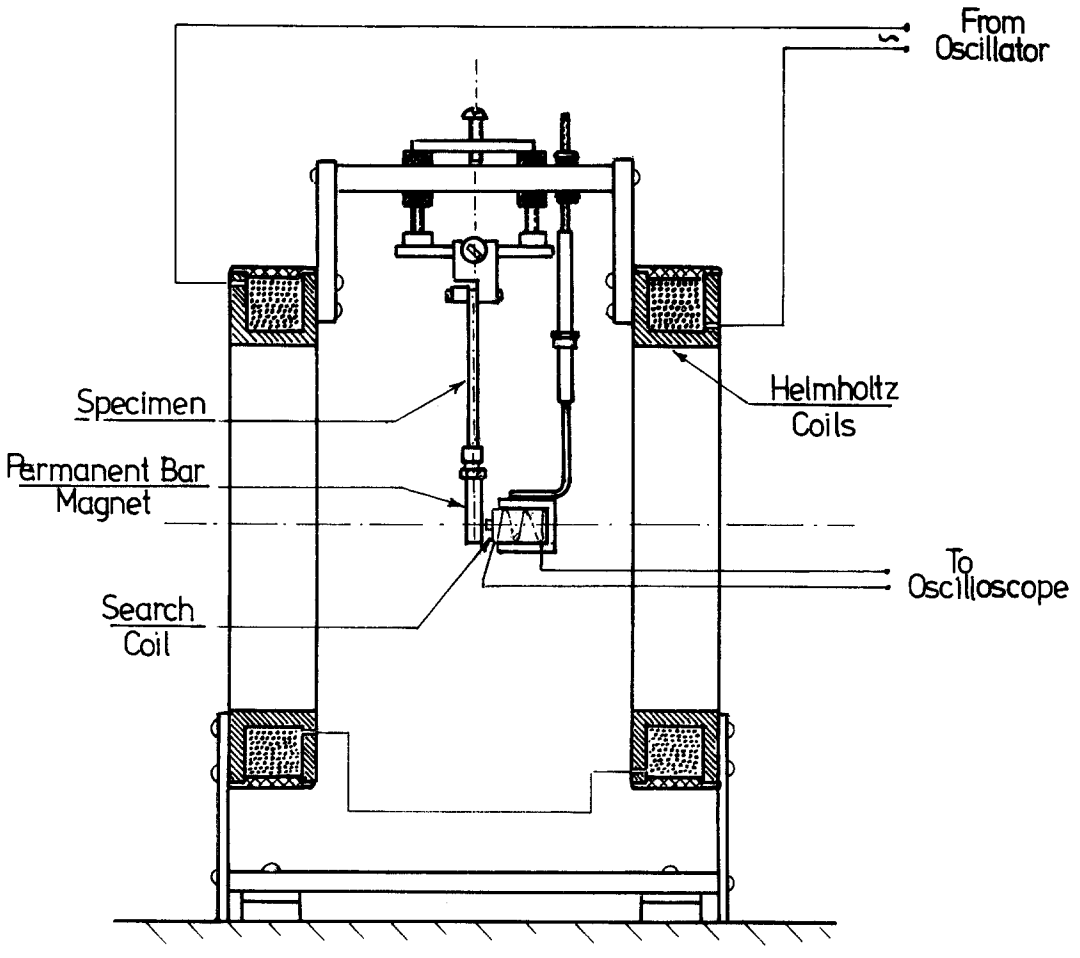

Figure 2 Diagrammatic sketch of the experimental set-up.

and

$$B = 1 + 4c + 12e + 12\frac{cL}{l} + 12\frac{cL^2}{l^2} - 12\frac{cgL}{l^2\omega^2}, \quad (9)$$

where e is I/m_0l^2, L is the distance of the centre of gravity of the load from the point of attachment of the load to the specimen, g is the acceleration due to gravity, c is the ratio of the mass of the load, M, to the mass of the specimen, m_0 and I is the moment of inertia of the load about an axis through the point of attachment of the load to the bar and perpendicular to the plane of motion.

To verify the accuracy of the present technique, specimens of pure aluminum (99.99% purity) and pure copper (99.95% purity) were tested. The measured Young's modulus values were 60.5 ± 1 GN m^{-2} and 130.9 ± 2 GN m^{-2} for the aluminum and copper, respectively. These values compare well with the values of 63 GN m^{-2} [20] and 125 GN m^{-2} [16] for aluminum and copper of comparable purity. An analysis of the experimental errors has shown that a 1% error in measuring the resonance frequency leads to a 2% error in the value of Young's modulus. Less serious errors arise from errors in the specimen length and density measurements. Young's modulus values were found to be relatively insensitive to errors in estimating the moment of inertia of the vibrating load.

3. Experimental results and discussion

As shown in Fig. 1, the alloys investigated in the present work can be classified into:

(i) Binary alloys of Al–Cu containing $CuAl_2(\theta)$-phase in a matrix of aluminum–copper solid solution (K-matrix), Fig. 3a; and Al–Ni containing ϵ-phase (Al_3Ni) in a matrix of almost pure Al, Fig. 3b.

(ii) Pseudobinary alloys containing τ-phase (Al_7Cu_4Ni) in a K-matrix, Fig. 3c; and δ-phase $(CuNi)_2Al_3$ in a K-matrix.

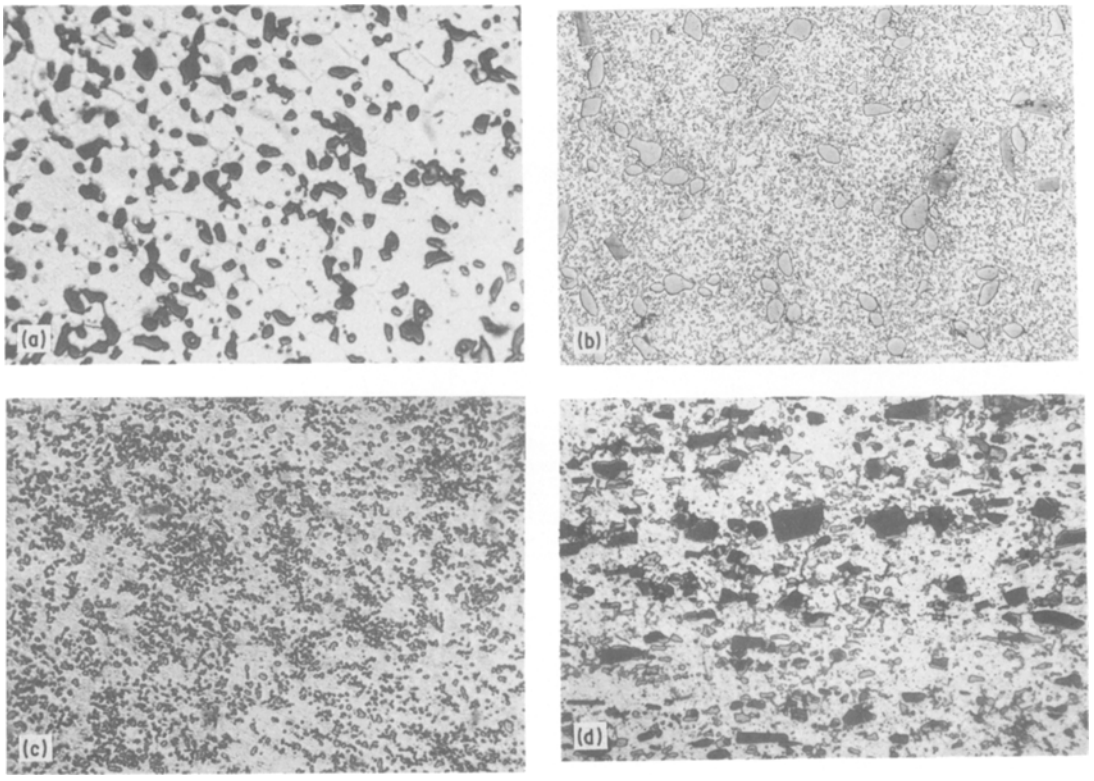

Figure 3 Typical microstructure of the alloys investigated: (a) Al–15 wt % Cu binary alloy, 20.17 vol % θ-phase in K-matrix, × 660; (b) Al–12.7 wt % Ni binary alloy, 25.08 vol % ϵ-phase in Al-matrix, × 435; (c) Al–10 wt % Cu–4 wt % Ni pseudobinary alloy, 31.5 vol % τ-phase in K-matrix, × 330; (d) Al–2 wt % Cu–7 wt % Ni three-phase alloy, 4.8 vol % ϵ-phase, 11.1 vol % δ-phase in K-matrix, × 500.

(iii) Three-phase alloys containing θ and τ-phases in a K-matrix, τ and δ-phases in a K-matrix; and ϵ and δ-phases in a K-matrix, Fig. 3d.

The variation of the different parameters of microstructure and their effect on the dynamic Young's modulus of the different alloys will be discussed in the following sections.

3.1. Al–Cu binary alloys

Generally, the Al–Cu alloys consisted of θ-phase particles dispersed within the K-matrix. The θ particles were of angular shape tending to elongate slightly as the Cu content increased in the alloy. The variation of the particle size, d, the inter-particle spacing, D, and the mean free path λ, with the percentage volume fraction of θ-phase, V_θ, is shown in Fig. 4.

The variation of the dynamic Young's modulus, E_c, with V_θ, Fig. 5, can be considered as the resultant of several opposing factors. Increasing V_θ is expected to increase E_c since E_θ is higher than E_k.

Lines 1, 2 and 3 of Fig. 5 represent the results of calculating E_c according to Equations 1, 2 and 3, taking the value of $E_\theta = 130\,\mathrm{GN\,m^{-2}}$ from [17] and the value of $E_k = 75\,\mathrm{GN\,m^{-2}}$, from the present results for Al–0.5 wt % Cu. The experimental values obtained at 1.9 and 4.7 vol % θ-phase exceeded the calculated upper boundary values. Young's modulus values that are higher than the upper boundary values are not uncommon in the literature, for example see [18], and are usually attributed to the constraint exerted on the matrix by the dispersed phase. Although the magnitude of the constraint cannot be calculated accurately, it is known to be a function of the ratio of mean free path to diameter and the ratio of the elastic properties of the matrix and particle [18]. In the case of the present results the ratio λ/d decreased from about 30, at 1.9 vol % θ-phase, to about 2.5, at 22 vol % θ-phase.

3.2. Al–Ni binary alloys

The microstructure of hypoeutectic alloys containing less than 6 wt % Ni consisted of fine, rounded particles of ϵ-phase in an almost pure

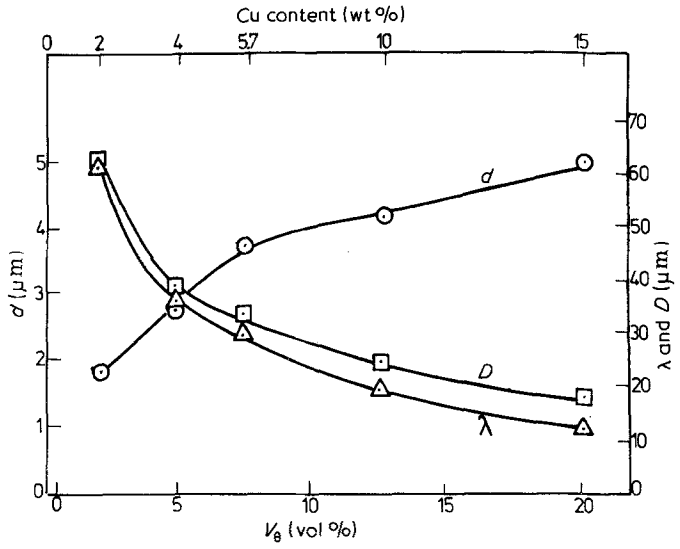

Figure 4 Variation of microstructural parameters with composition for binary Al–Cu alloys. d is the particle size of the θ-phase, λ is the mean free path, and D is the interparticle spacing.

aluminium matrix. The hypereutectic alloys contained coarse angular primary ϵ-phase in a eutectic matrix, Fig. 3b. The variation of ϵ-phase particle size, d, mean free path, λ, and interparticle spacing, D, with the percentage volume fraction of ϵ-phase in the alloy, V_ϵ, is shown in Fig. 6.

The variation of the dynamic Young's modulus with the volume fraction of the ϵ-phase, V_ϵ, is shown in Fig. 7 together with the calculated lines from Equations 1, 2 and 3. For the calculations, E_ϵ was taken as $215\,\mathrm{GN\,m^{-2}}$, from [19], and E_{Al} was taken as $65\,\mathrm{GN\,m^{-2}}$, from the present results. Up to the eutectic composition, the experimental results of Young's modulus fall very close to the calculated upper boundary values. The appearance of the massive primary ϵ-phase in the hypereutectic alloys causes a noticeable decrease in the Young's modulus values. This decrease could have been partly caused by cracking of the large intermetallic compounds during specimen preparation by swaging, Fig. 8.

3.3. $K-\tau$ pseudobinary alloys

The structure of the $K-\tau$ pseudobinary alloys consisted of fine angular particles of τ-phase in K-matrix. The variation of the τ-phase particle size, d, interparticle spacing, D, and mean free path, λ, with the percentage volume fraction of the τ-phase is shown in Fig. 9. As in the case of $K-\tau$ binary alloys, increasing the τ-phase fraction increases the value of E_c, as shown in Fig. 10.

An approximate value of E_τ was estimated by drawing a line to pass through the highest E_c points of Fig. 10, Line 1 and extrapolating to 100 vol% τ-phase. The estimated value of E_τ is $163\,\mathrm{GN\,m^{-2}}$. This value was substituted into Equations 2 and 3 to obtain Lines 2 and 3 of Fig. 10. Most of the experimental points fall within the area between Lines 1 and 3. However,

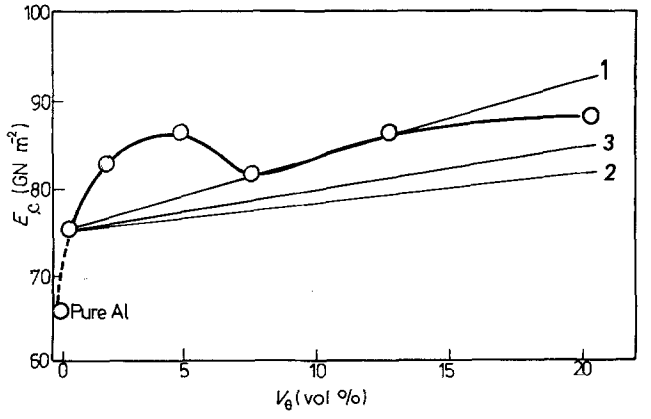

Figure 5 Variation of Young's modulus with vol% of the θ-phase, V_θ for binary Al–Cu alloys. Lines 1, 2 and 3 are calculated according to Equations 1, 2 and 3, respectively.

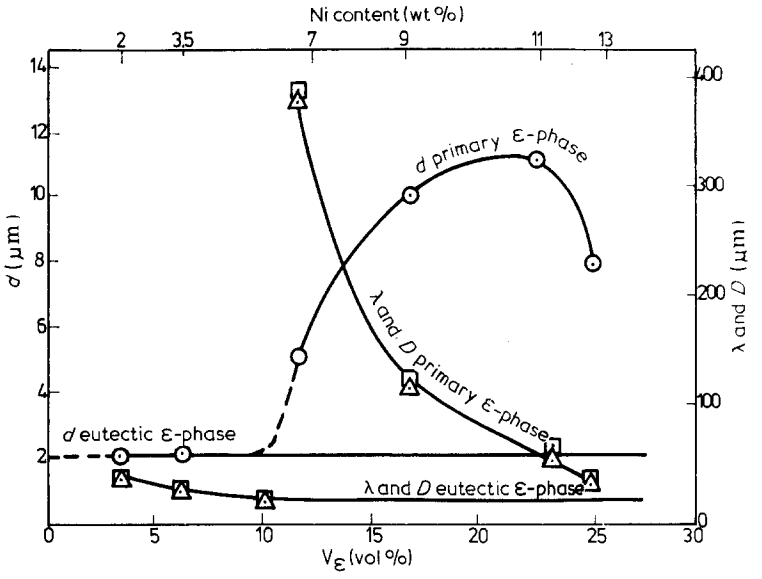

Figure 6 Variation of microstructural parameters with composition for binary Al–Ni alloys. d is the particle size of the ϵ-phase, λ is the mean free path, and D is the interparticle spacing.

the Young's modulus value of the alloy containing 10 vol% τ-phase is abnormally low, which could be attributed to the combined effect of relatively large value of d and low volume fraction of τ-phase.

3.4. $K-\delta$ pseudobinary alloys

The structure of the $K-\delta$ pseudobinary alloys was similar to the $K-\tau$ structure and consisted of fine angular particles of δ-phase in a K-matrix. The variation of the δ-phase, particle size, d, interparticle spacing, D, and mean free path, λ, with percentage volume fraction of the δ-phase is shown in Fig. 11. The Young's modulus progressively increased with increasing δ-phase vol% up to about 22 vol%, Fig. 12. The appearance of massive δ-phase particles in the 5.7 wt% Cu–8 wt% Ni alloy caused a noticeable decrease in the Young's modulus values. Microscopic examinations showed cracks in the δ-phase similar to those shown in Fig. 8.

An approximate value of E_δ was estimated by drawing a line to pass through the highest E_c points of Fig. 12, Line 1, and extrapolating to 100 vol% δ-phase; The estimated value of E_δ is 185 GN m^{-2}. This value was substituted in Equations 2 and 3 to obtain Lines 2 and 3 of Fig. 12. All the experimental points fall within the area between Lines 2 and 3 except for the case where cracked δ-phase was observed.

3.5. Three-phase alloys

The three-phase alloys investigated in the present work can be grouped into 3 types: $K-\theta-\tau$, $K-\tau-\delta$, and $K-\delta-\epsilon$. In most cases, the microstructure consisted of independently dispersed phases in the K-matrix. In some cases, especially in

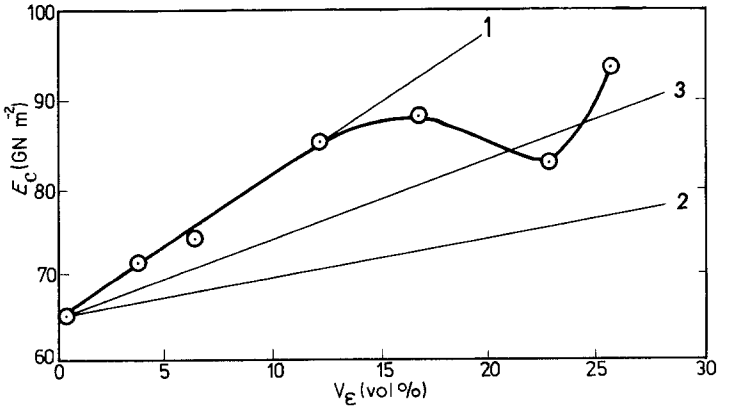

Figure 7 Variation of Young's modulus with vol% of the ϵ-phase, V_ϵ, for binary Al–Ni alloys. Lines 1, 2 and 3 are calculated according to Equations 1, 2 and 3, respectively.

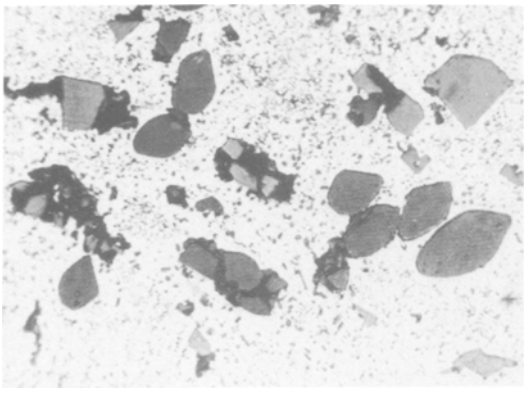

Figure 8 Cracks in massive primary ϵ-phase in a binary Al–Ni alloy containing 11 wt% Ni and 22.5 vol% ϵ-phase.

the $K-\tau-\delta$ system, some of the δ-phase particles were enveloped completely or partially within the τ-phase particles. The particle sizes in the different three-phase alloys is shown in Table I. The mean free path and interparticle spacing were calculated from the total volume fraction and average particle size of the dispersed phases irrespective of their type, see Table I.

The experimentally measured values of E_c are given in Table I together with the estimated values of the upper and lower limits (UL and LL) calculated from Equations 1 and 2, respectively. For the calculations, the Young's modulus values of the different phases were taken as $E_k = 75\,GN\,m^{-2}$, $E_\tau = 163\,GN\,m^{-2}$, $E_\delta = 180\,GN\,m^{-2}$, $E_\theta = 130\,GN\,m^{-2}$, $E_\epsilon = 215\,GN\,m^{-2}$. The first three values are estimated from the present work and the last two values are taken from [17] and [19], respectively.

Generally the Young's moduli of the alloys containing fine dispersions fall close to the upper boundary values while those containing coarser dispersions fall between the upper and lower boundary values.

4. General discussion and conclusion

The equi-modulus contours of Fig. 13 summarize the results obtained in the present work. This figure was obtained by writing the Young's modulus values in the appropriate places on the equilibrium diagram and then joining the compositions of equal Young's moduli with an equi-modulus contour; the technique of linear interpolation was used. In spite of the fact that ϵ-phase has the highest modulus of the intermetallic compounds studied in this work, the alloys which exhibited the highest modulus did not contain this phase. Fig. 13 shows that compositions with highest modulus fall in the areas of $K+\theta+\tau$, $K+\tau$, and $K+\tau+\delta$. This supports the idea that the composition is not the only parameter which determines the Young's modulus of an alloy; the microstructure plays an important role in determining the value of the Young's modulus.

A linear multiple regression analysis of the results corresponding to sound microstructures was carried out and the following simple relationship was found to have a correlation coefficient of 0.88 which indicates reasonable accuracy:

$$E = 76.6 + 94.6\,V_d - 1.3d + 0.06\lambda \quad (10)$$

where E is Young's modulus of the alloy (in $GN\,m^{-2}$), V_d is the sum of the volume fractions of all the dispersed phases of the alloy, d and λ

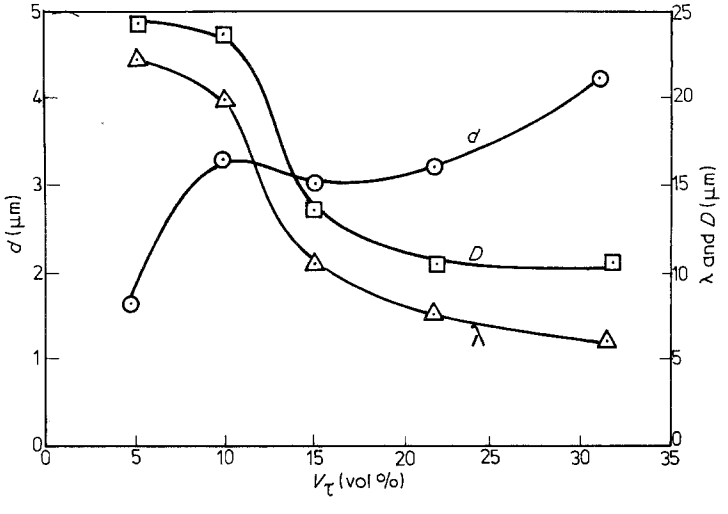

Figure 9 Variation of microstructural parameters with τ-phase vol%, V_τ, for $K-\tau$ pseudobinary alloys. d is particle size of the τ-phase, λ is the mean free path, and D is the interparticle spacing.

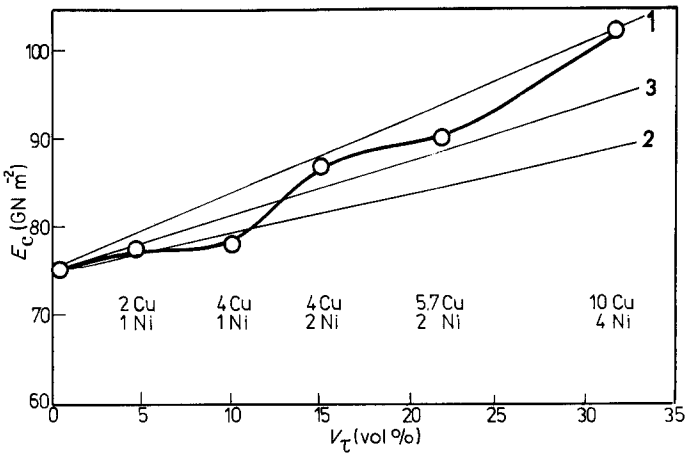

Figure 10 Variation of Young's modulus with τ-phase vol%, V_τ, for $K-\tau$ pseudobinary alloys. Lines 2 and 3 are calculated according to Equations 2 and 3, respectively.

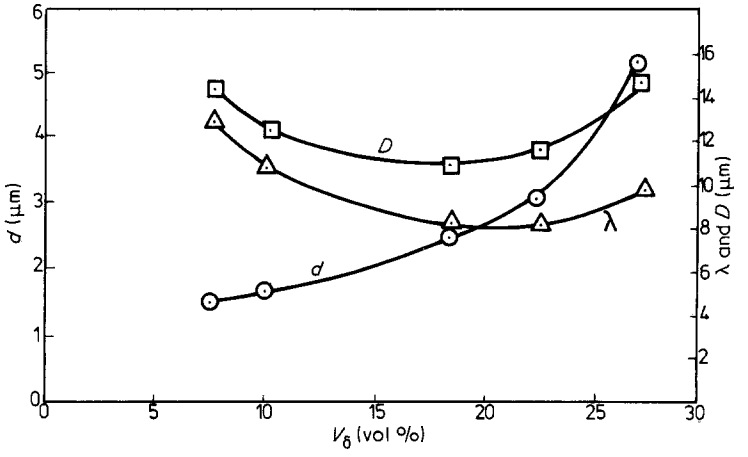

Figure 11 Variation of microstructural parameters with δ-phase vol%, V_δ, for $K-\tau$ pseudobinary alloys. d is the particle size of the δ-phase, λ is the mean free path, and D is the interparticle spacing.

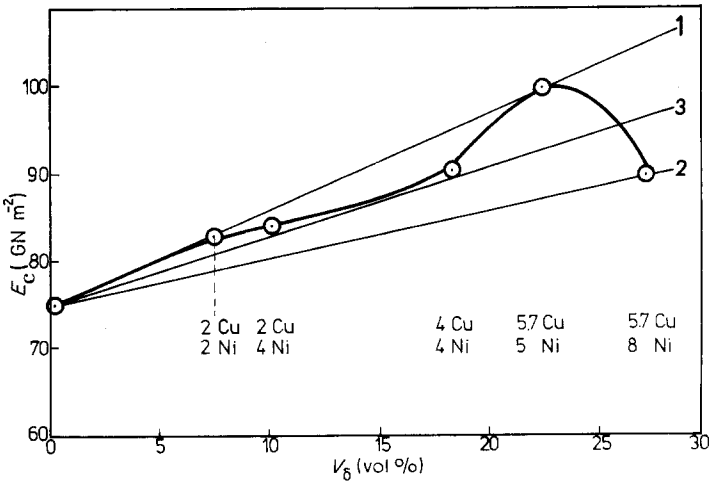

Figure 12 Variation of Young's modulus with δ-phase vol%, V_δ, for $K-\delta$ pseudobinary alloys. Lines 2 and 3 are calculated according to Equations 2 and 3, respectively.

TABLE I Microstructural parameters and Young's modulus of three-phase alloys

Nominal alloy addition		Type of dispersion		Volume fraction (%)		Particle size (μm)		λ (μm)	D (μm)	E_c (GN m^{-2})		
										Expt*	U.L.†	L.L.‡
Ni (wt%)	Cu (wt%)	Phase 1	Phase 2	Phase 1	Phase 2	Phase 1	Phase 2					
1	5.7	θ	τ	10	5.7	1.9	1.0	5.2	6.7	84.5	85.4	81.2
2	10	θ	τ	3.9	17.8	3.0	3.8	8.1	11.5	95.0	92.8	84.4
3	15	θ	τ	7.1	28.9	3.5	4.1	4.5	8.3	104.9	104.3	92.1
6	1	ϵ	δ	12.5	3.5	1.5	1.2	4.7	6.1	97.0	96.4	83.5
7	2	ϵ	δ	4.8	11.1	3.6	1.3	8.6	11.0	95.5	93.8	83.2
8	2	ϵ	δ	9.5	10.0	1.8	1.5	4.5	6.2	94.0	98.8	85.2
9	2.5	ϵ	δ	4.3	19.5	5.0	1.9	7.4	10.8	94.0	102.0	86.7
5	10	τ	δ	28.5	1.7	5.5	2.5	6.2	10.2	94.0	102.0	89.7
6	8	τ	δ	0.9	16.0	7.5	1.5	14.7	19.2	93.0	93.4	83.0
7	14	τ	δ	42.5	0.25	4.8	3.7	3.8	8.0	98.5	112.6	97.5
8	10	τ	δ	4.5	25.5	11.6	22.0	26.1	42.9	93.0	105.7	88.8

*Experimental result.
†Upper limit.
‡Lower limit.

are respectively the average particle size and mean free path of all dispersed phases (given in μm). An advantage of Equation 10 is that the knowledge of the Young's modulus of the individual phases is not needed in order to predict the Young's modulus of the alloy. In view of the wide range of alloys tested in the present work, Equation 10 is expected to apply reasonably well to most wrought aluminum alloys.

A more detailed relationship was also attempted:

$$E = E_m V_m + E_\theta V_\theta + E_\epsilon V_\epsilon + E_\tau V_\tau + E_\delta V_\delta - 0.67d + 0.16\lambda, \quad (11)$$

where E_m, E_θ, E_ϵ, E_τ, and E_δ are the Young's moduli (in GN m^{-2}) of the matrix θ-, ϵ-, τ- and δ-phases, respectively and V_m, V_θ, V_ϵ, V_τ, and V_δ are the volume fractions of the matrix, θ-, ϵ-, τ- and δ-phases, respectively. Equation 11 has the advantage of specifying the different phases in the alloy and can be considered as a modification of

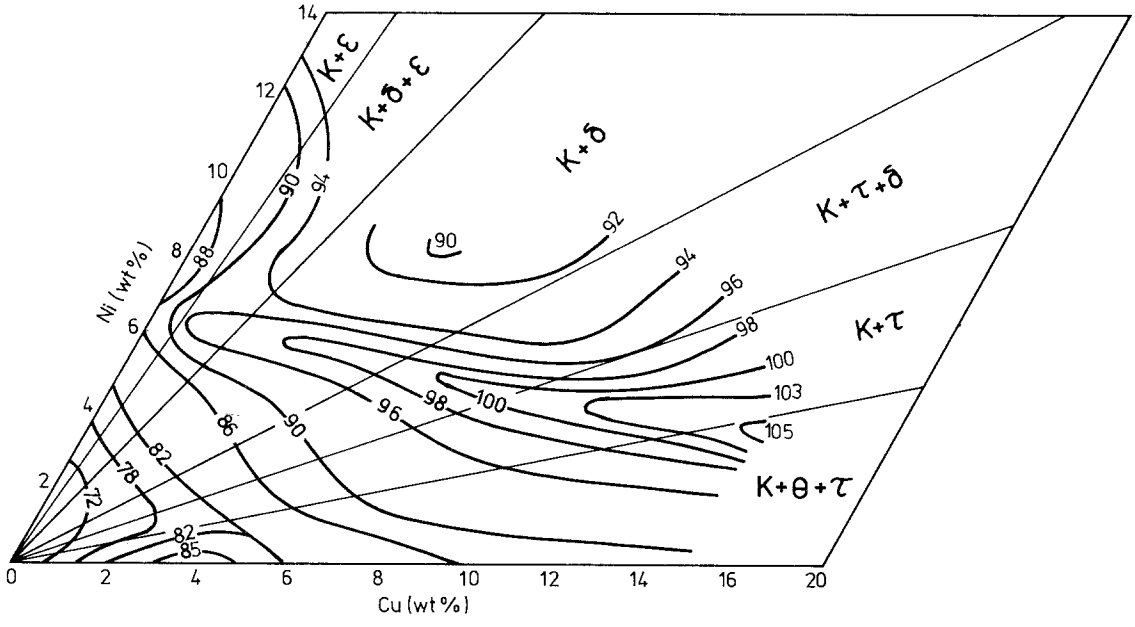

Figure 13 Equi-modulus contours for wrought Al–Cu–Ni alloys.

the rule of mixtures, Equation 1. However, the correlation coefficient of Equation 11 is only 0.59 which indicates a lower accuracy than Equation 10. This relatively low correlation coefficient is caused by the large number of parameters involved in Equation 11.

References

1. W. KOSTER and W. RAUSCHER, *Z. Metallkde* **39** (1948) 111.
2. S. UMEKAWA and O. D. SHERBY, *J. Mech. Phys. Sol.* **14** (1966) 63.
3. B. SUBRAHMANYAM, *Trans. JIM* **13** (1972) 89.
4. *Idem, ibid.* **13** (1972) 93.
5. *Idem, Mater. Sci. Eng.* **12** (1973) 187.
6. Y. C. WAUNG, D. E. BESKOS and W. SACHSE, *J. Mater. Sci.* **10** (1975) 109.
7. W. KOSTER and H. FRANZ, *Met. Rev.* **6** (1961) 29.
8. F. Y. WANG, *Mater. Sci. Eng.* **7** (1971) 110.
9. R. C. ROSSI, *J. Amer. Ceram. Soc.* **51** (1968) 433.
10. Z. HASHIN, *Trans. ASME J. Appl. Mech.* **29** (1962) 143.
11. B. PAUL, *Trans. Metall. Soc. AIME* **218** (1960) 36.
12. K. OGAWA, F. FUKUDA and K. IWAMOTO, *J. Mater. Sci.* **11** (1976) 1362.
13. R. FARRARO and R. B. McLELLAN, *Met. Trans. A* **8A** (1977) 1563.
14. C. J. MARTIN and V. A. PHILLIPS, *Mater. Sci. Eng.* **30** (1977) 81.
15. J. H. TREJILGAS and T. Z. KATTAMIS, *J. Mater. Sci.* **11** (1976) 1239.
16. K. D. BAVEJA, *J. Sci. Instruments* **41** (1964) 662.
17. Y. C. WAUNG, D. E. BESKOS and W. SACHSE, *J. Mater. Sci.* **10** (1975) 109.
18. R. H. KROCK and L. J. BROUTMAN, "Modern Composite Materials" (Addison-Wesley, New York, 1967) p. 13.
19. J. V. GRABEL and J. R. COST, *Met. Trans.* **3** (1972) 1973.
20. L. E. MONDOLFO, "Aluminium Alloys: Structure and Properties" (Butterworth and Co., London, 1976) p. 81.

Received 2 May and accepted 17 October 1980.